JOURNAL OF Applied Polymer SCIENCE

Study on single and binary catalytic systems of pyridine-imine catalysts based on nickel and iron in synthesis of reactor blends and low-density polyethylene nanocomposites

Mohsen Mogheiseh,[1] **Gholam Hossein Zohuri**,[1,2] **Mostafa Khoshsefat**[3,4]

[1]Department of Chemistry, Faculty of Science, Ferdowsi University of Mashhad, PO Box 91775-1436, Mashhad, Iran
[2]Environmental Chemistry Research Centre, Department of Chemistry, Faculty of Science, Ferdowsi University of Mashhad, PO Box 91775-1436, Mashhad, Iran
[3]Department of Catalyst, Iran Polymer and Petrochemical Institute (IPPI), PO Box 14965/115, Tehran, Iran
[4]Department of Chemical and Materials Engineering, University of Alberta, Edmonton, Alberta T6G 1H9, Canada
Correspondence to: G. H. Zohuri (E-mail: zohuri@um.ac.ir)

ABSTRACT: In the presence of modified methylaluminoxane as cocatalyst, the behavior of a binary catalytic system based on pyridine-imine nickel (**N**) and iron (**F**) catalysts was evaluated in order to reach a proper mixture of polyethylene (PE). A computational study along with kinetic profile suggested that the catalyst **F** with higher electron affinity (*A*) and electrophilicity (ω) in the methyl cationic active center and stronger interaction with the monomer led to high integrated monomer consumption and higher activity. In addition, the samples produced by the mixture of catalysts showed a higher value of $\overline{M}_v$ [19.4×10^4 g (PE) mol $(Fe+Ni)^{-1}$ h^{-1})], melting point (127.8 °C), and crystallinity extent (41.29%) than the samples produced by the single catalysts. The addition of multiwalled carbon nanotubes (MWCNT) into the polymerization media reduced the activity of catalysts [from 7.50×10^4 to 0.66×10^4 g (PE) mol $(Fe+Ni)^{-1}$ h^{-1}] and the thermal properties of the low-density polyethylene nanocomposite samples. However, the sample containing 2.33% $MWCNT_{20\text{-}30}$ improved the total thermal stability of the neat polyethylene blend up to 400 °C. Scanning electron microscope images of the samples demonstrated irregular to virtually uniform morphologies were obtained through the *in situ* and solution-mixing techniques. © 2019 Wiley Periodicals, Inc. J. Appl. Polym. Sci. **2019**, *136*, 47376.

KEYWORDS: catalysts; composites; polyolefins

Received 29 May 2018; accepted 4 November 2018
DOI: 10.1002/app.47376

INTRODUCTION

Polyethylene (PE) is a low-cost, multipurpose thermoplastic with high production volume that shows good mechanical properties and high chemical resistance. For PE, blending is primarily applied to control the balance between processability and the mechanical properties of the raw materials.[1,2] Basically, polyolefin blends are obtained by four methods: mixing by an extruder under determined conditions, polymerization in multistage reactors, utilization of operating conditions,[3–5] and obtaining favored microstructures of polyethylene blends by a specific combination of different catalysts. Up to now, various types of catalyst combinations, including Ziegler–Natta/metallocene, Ziegler–Natta/late transition metals (LTM), metallocene/metallocene, metallocene/LTM, and finally LTM/LTM have been studied in (co)polymerization of different types of monomers to produce ideal reactor polymer blends.[3,4,6–12]

Nowadays, regarding choosing a type of catalyst for polymerization of ethylene leading to a polymer with a specific microstructure, using a binary catalytic system is vast and interestingly, based on the features and applications of resultant blends, it could be diverse. Hence, it is obvious that the appropriate conditions for polymerization of ethylene in addition to specific features of additives play key roles in the engineering of nanocomposite/polyolefin blends.[13,14]

Various types of additives as well as different sizes of particles can be used to prepare the composites. Carbon nanotubes (CNTs) as effective additives have attracted much interest from academics and industries because of their outstanding mechanical, thermal, and electrical properties. The CNTs tend to form clusters and bundles due to van der Waals forces and strong π-π interactions between the tubes, which can be used to improve the

Additional Supporting Information may be found in the online version of this article.

interfacial adhesion between polyolefin matrixes. Applications of these materials are being studied in a wide range of areas, from construction to automotive and aerospace engineering, alternative energy production, and medicine. Much attention has been paid to CNT-based nanocomposites for the preparation of high-performance materials that exhibit improved or unusual mechanical and physical properties, even at very low nanofiller loading.[15,16] In this field, many studies[17–20] have focused on utilizing specific methods to produce polymer nanocomposites. Three methods are mainly used to incorporate CNTs into polymer composites: (1) "Polymerization-filling technology (PFT)," which is a promising approach for the preparation of polyolefin nanocomposites that includes the growth of chains directly on the surface of the catalyst that are attached to the fillers. Therefore, *in situ* polymerization can make nanocomposites with a much more uniform filler dispersion and strong interfacial adhesion without damaging filler structures (such as CNTs and graphene).[21–28] The product may be used directly as a masterbatch for future nanocomposites.[29,30] (2) Film casting from a suspension of CNTs in a polymer solution, which through vigorous mixing may lead to serious defects in the nanotube structure and may hinder their unique properties.[31,32] (3) Postpolymerization mixing of the polymer with different sizes of filler in an extruder under determined conditions.[33–36]

Melt and solution blending are methods frequently used to prepare polymer nanocomposites, and under these conditions the homogeneous dispersion of CNTs within a polymeric matrix, especially apolar matrixes (such as polyolefins), is relatively difficult to achieve. Therefore, a key factor to achieve appropriate products consists of breaking down the native bundles of the CNTs to reach a high level of nanofiller dissociation and establish a strong CNT–polymer interfacial adhesion for a good load transfer.[37,38] Here, we report the synthesis and characterization of pyridine-imine catalysts based on nickel and iron, and we study single and binary catalyst systems in the polymerization of ethylene to reach an ideal blend at the desired conditions. Therefore, the effects of composition and type of catalysts on the microstructure of the product were evaluated. Furthermore, we investigated the mutual effect of catalyst and CNTs in regard to the catalytic system used and CNT size through the *in situ* polymerization method. Moreover, the solution-mixing method was employed for comparison. Therefore, the influence of type and content of CNTs, the method applied on catalyst behavior, and the low-density polyethylene (LDPE)/multiwalled carbon nanotube (MWCNT) nanocomposite properties (thermal, physical, and morphological) are further discussed in detail.

EXPERIMENTAL

Materials and Methods

All procedures that included air- or moisture-sensitive compounds were performed under an inert and dry atmosphere in a glove box or under ultrapure argon protection. The equipment and solvents (supplied by Merck Chemicals (Darmstadt, Germany)) were dried before use. Toluene (Iran, Petrochemical Co.), diethyl ether (DEE), and tetrahydrofuran (THF) were dried over Na/benzophenone and distilled. Similar equipment was employed in the purification of dichloromethane (DCM), and CaH_2 was used as a drying agent for *n*-hexane. Methanol was dried by refluxing in the presence of Mg/iodine (drying agent), distilled, and kept on an active molecular sieve type 3Å/13X. Ethylene (polymerization grade) (Iran, Petrochemical Co.) was dried by passing through an activated molecular sieve column. 2-Acetylpyridine, dimethoxyethanenickel dibromide (DME) $NiBr_2$, anhydrous iron (II) chloride, decaline, chlorobenzene, and CaH_2 were purchased from Sigma Aldrich Chemical (St. Louis, MO). $MWCNT_{20\text{-}30}$ (with an outside diameter of 20–30 nm, a length of 10–30 μm, and true density of 2.1 g cm^{-3}) and $MWCNT_{30\text{-}50}$ (with an outside diameter of 30–50 nm, a length of 10–20 μm, and true density of 2.1 g cm^{-3}) were purchased from US Research Nanomaterials (Houston, TX) and used without any further purification. Triisobutylaluminum also was supplied by Sigma-Aldrich (Steinem, Germany) Chemical and was used in the synthesis of modified methylaluminoxane (MMAO) according to the literature.[39]

Synthesis and Characterization of Ligand and Catalysts

Synthesis of 2-((2,6-Diisopropylphenylimino)ethyl)pyridine (L). The ligand (L) was prepared through a procedure similar to that reported in the literature.[40] A mixture of the appropriate 2-acetylpyridine compound (21.5 mmol), 2,6-diisopropylaniline (28.7 mmol), a catalytic amount of formic acid (3 drops), and sodium sulfate in methanol (30 mL) was refluxed for 7 h. After cooling to room temperature, the precipitate was removed by filtration. The residue was kept in the freezer, and after 24 h, yellowish crystals appeared. The crystals were collected and washed with cold methanol to remove unreacted reactants. The product was dried under vacuum for characterization and preparation of the catalyst.

Formula $C_{19}H_{24}N_2$, MW = 280.41 g mol^{-1}; ^{1}H-NMR (300 MHz, $CDCl_3$, δ, ppm): 1.17 (12H, d), 2.24 (3H, s), 2.78 (2H, m), 7.10–7.21 (3H, m), 7.42 (1H, t), 7.84 (1H, t), 8.37 (1H, d), 8.72 (1H, d). ^{13}C-NMR (300 MHz, $CDCl_3$, selected δ, ppm): 167.01 (C(Me)═N), 156.47, 148.62, 146.44, 136.53, 135.81, 124.84, 123.64, 123.03, 121.36, 28.29, 28.06, 23.27, 22.96, 17.38. FTIR (KBr, cm^{-1}): 3060, 2957, 1636, 1584, 1465, 1363, 1240, 1104, 775. MS (EI, m/z): 280 [M^+]. Elemental analysis calculation: C, 81.38; H, 8.63; N, 9.99; found: C, 82.79; H, 8.83; N, 9.96.

Preparation of the Catalyst 2-((2,6-Diisopropylphenylimino) ethyl)pyridine nickel dibromide (N). A suspension of [$NiBr_2$(DME)] (0.31 mmol) in dichloromethane (20 mL) was treated with a solution of 2-[(2,6-dibenzhydryl-4-methylphenylimino)methyl]pyridine (0.31 mmol) in dichloromethane (10 mL) in a glove box. The mixture was stirred at room temperature for 24 h, filtered, and the solvent was evaporated. The crude product was washed with DEE several times and dried in vacuum. The yield of the reaction was about 90%.

Formula $C_{19}H_{24}Br_2N_2Ni$, MW = 498.91 g mol^{-1}; FTIR (KBr, cm^{-1}): 3076, 2965, 1617, 1590, 1446, 1321, 1180, 781. Elemental analysis calculation: C, 45.74; H, 4.85; N, 5.61; found: C, 45.07; H, 4.45; N, 5.14.

Preparation of the Catalyst 2-((2,6-Diisopropylphenylimino) ethyl)pyridine iron dichloride (F). To a suspension of anhydrous $FeCl_2$ (0.31 mmol) in THF (20 mL) at 70 °C a solution of 2-[(2,6-dibenzhydryl-4-methylphenylimino)methyl]pyridine (0.31 mmol)

in THF (10 mL) was added. The resulting mixture was stirred for 2 h, filtered, and its solvent was evaporated. The crude product was washed with dry *n*-hexane and diethyl ether and dried under inert atmosphere in a glove box. The product was obtained as a dark red powder, and the yield of the reaction was about 73%.

Formula $C_{38}H_{48}Cl_4Fe_2N_4$, MW = 814.32 g mol^{-1}; FTIR (KBr, cm^{-1}): 3084, 2964, 1619, 1592, 1441, 1317, 1186, 782. Elemental analysis calculation: C, 56.05; H, 5.94; N, 6.88. Found: C, 55.71; H, 5.48; N, 6.52.

General Procedure for Ethylene Polymerization

The polymerization of ethylene was performed in a sealed glass reactor equipped with a Schlenk system, ethylene inlet, and magnetic stirrer. The reactor was degassed and filled with monomer several times to remove oxygen and moisture. The desired amount of MMAO was introduced into toluene (solvent) under the continuous pressure of ethylene. An ice bath was used in order to control the temperature at 0 °C. Afterward, toluene and cocatalyst (MMAO) were injected into the reactor, successively. Polymerization was initiated by injecting an appropriate amount of the catalyst(s) (10 μmol) into the reactor. The reaction temperature and ethylene pressure were kept constant during the polymerization process. At the end of polymerization, the remaining monomer was vented, and the reaction was quenched by acidified methanol (5% v/v). The solid polyethylene was filtered and washed with methanol and dried under reduced pressure.[10,27]

Procedures for Preparation of LDPE/MWCNT Nanocomposites

For *in situ* polymerization, a specific amount and type of MWCNT was added to a round-bottom flask containing toluene to disperse the particles. The mixture was injected into the polymerization reactor before addition of the catalyst(s) (5–10 min). The reaction was carried out for 3 h, and the reaction was vented and then quenched by adding the acidified methanol. The product was then filtered and dried under reduced pressure (40 °C).

For solution mixing, to a clear solution of LDPE in toluene at 80 °C under vigorous stirring (1500 rpm), a prescribed amount of MWCNT was added, and the final mixture was stirred while heating with a mild heating rate up to 100 °C. The hot, homogenized mixture was quenched by pouring it into a glass dish at room temperature. After 24 h, the solvent was evaporated, and a composite film was obtained.[2,31,32]

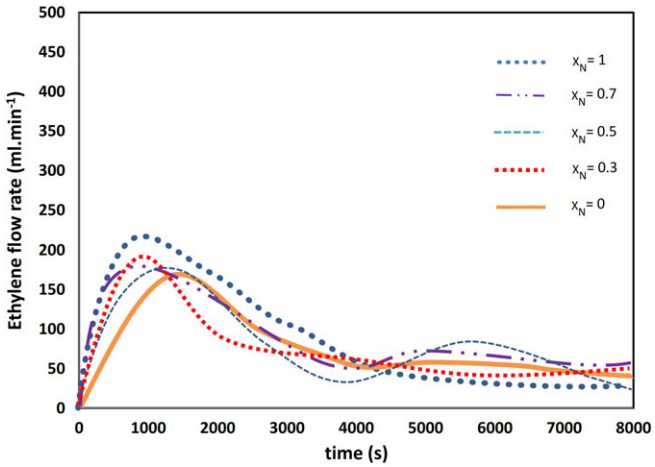

Figure 1. Kinetic profile of ethylene polymerization with different ratios of catalyst **N** (X_N) in the N/F/MMAO binary system. [Color figure can be viewed at wileyonlinelibrary.com]

Characterization

^{1}H-NMR and ^{13}C-NMR mass spectra and elemental analysis were recorded using Bruker Avance III-300 (Karlsruhe, Germany) and Varian CH-7A spectrometers (Palo Alto, CA) and a Thermo Finnigan Flash 1112EA microanalyzer (Waltham, MA), respectively. The Fourier transform infrared (FTIR) spectra (resolution of 5 at 32 runs) were recorded using a Thermo Nicolet AVATAR 370 (Waltham, MA) to determine the vinyl and branching content, which were calculated according to our previous work.[40,41] The viscosity average molecular weight (M_v) of the polymer samples was determined according to the literature ($[\eta] = 6.2 \times 10^{-4} M_v^{0.7}$, where [η] is intrinsic viscosity, α (0.7) and k (6.2×10^{-4}) are mark-houwink constants).[40] Thermogravimetric analysis (TGA; PerkinElmer TGA-7, Waltham, MA) and differential scanning calorimeter (DSC) instruments (Mettler Toledo DSC822, Columbus, OH) with a constant rate of 10 °C/min were used for polyethylene and nanocomposite characterization. The degree of crystallinity of the samples was calculated from the heat of fusion determined by DSC.[42] The scanning electron microscope (SEM) images were obtained using a LEO VP 1450 instrument (Zeiss, Oberkochen, Germany).

RESULTS AND DISCUSSION

Computational Study

By considering the kinetic profile of the ethylene polymerization using single and binary catalyst systems, different trends in regard to activation and monomer insertion can be observed (Figure 1). To find the effect of molecular structure on the catalyst behavior, a series of theoretical studies were carried out. The precatalyst structures were built at the ground state according to the single-crystal monostructures provided in the literature.[43,44] Methyl cationic active centers (MCC) and ethylene π–complexes (π-comp.) were optimized using the Density Functional Theory (DFT) method at the B3LYP level using a 6-31+G basis set (Figure 2) by Gaussian 09W. In the structure of the Ni catalysts ($LNiX_2$), bromide atoms (X═Br) show greater activity than chloride (X═Cl) according to the literature, and also for a similar comparison, the precatalyst structures were considered for both halogen atoms.[45,46] Based on the computational results, the higher activity of the bromide structure can be attributed to the lower M—X bond dissociation energy for Ni—Br (360.0 kcal/mol) than for Ni—Cl (372.3 kcal/mol). Moreover, the higher electron affinity (*A*), global electrophilicity (ω), and lower chemical hardness (η) in the precatalyst, the closer match of Ni—Br bond dissociation energy to Al—C (267.7 kcal/mol), and the greater stability of the ethylene π–complex (stronger interaction of Ni and ethylene monomer) can lead to faster activation and a steep slope at the beginning of the kinetic profile (Table I). However, total activity of the catalyst **F** was higher than that of catalyst **N** due to higher mentioned theoretical parameters (*A* and ω), along with the Mulliken charge on the metal center in the π–complex affording a higher monomer uptake during the propagation reaction. More efficient

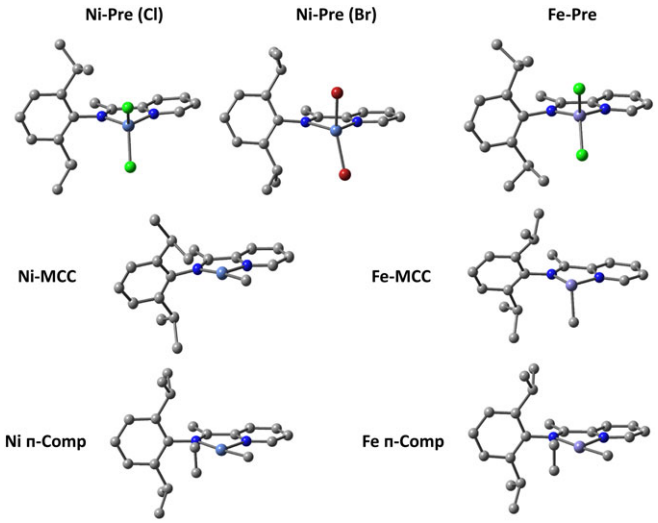

Figure 2. Molecular structures of Ni and Fe precatalysts, methyl cationic active centers, and ethylene π-complexes. [Color figure can be viewed at wileyonlinelibrary.com]

shielding of the axial sites in the coordination planes (*xy*, *xz*, *yz*) of the catalyst **F** containing an Fe cationic center, on the other hand, is another reason for the higher stability and performance of the catalyst **F** (Figures 3 and 4). As can be observed, the electron density around the Fe active center, especially in the planes *xz* and *yz* (axial sites), is higher than for Ni. The kinetic profile for each molar ratio of the catalysts is consistent with this explanation.

Thermal and Structural Analysis

Our previous studies have demonstrated that pyridine-imine catalysts are active for producing low-density polyethylene. In addition, using the single catalytic system of each one only yields a low-molecular-weight polyethylene, which dramatically depends on the polymerization parameters (the results for both catalysts are tabulated in the Supporting Information).[40,47] In the present work, initially, polyethylene reactor blends were prepared using a binary system of the catalysts at different ratios of the complexes, and the results as well as the reaction conditions are tabulated in Table II. As can be observed, both catalysts had high activity in the single system at 0 °C. However, at the same polymerization conditions, the catalyst system N/MMAO showed a lower catalytic activity and $\overline{M}_v$ of the PE in comparison to F/MMAO (entries 1 and 5, Table II). The obtained results indicated that not only the polymerization activities but also the $\overline{M}_v$, melting temperature, crystallinity extent, and branching density of the polyethylene blends varied with the change in molar fraction of catalyst **F** (X_F) used in the reaction. Therefore, the catalytic activity using the binary system decreased linearly with increasing molar fraction of the catalyst **N** (X_N) [from 33.33 to 3.50 × 10^4 g (PE) mol (Ni+Fe)$^{-1}$ h^{-1}]. This observation can be attributed to the minimum interaction of catalysts **N** and **F** regarding the activity and selective activation of the metallic centers in the applied catalyst system during the ethylene polymerization (Table II).[10,48] The $\overline{M}_v$ values of the polyethylene blends obtained at a fixed [Al]/[Ni+Fe] ratio for each run had much

Table I. Theoretical Calculated Parameters at Different States of Ni and Fe Species

Parameters	Ni-Pre (Br)	Ni-Pre (Cl)	Ni-MCC	Ni π-comp.	Fe-Pre	Fe-MCC	Fe π-comp.
Energy (e.u.)	−7504.2402	−3276.4236	−2395.6513	−2474.2624	−3031.9352	−2151.1080	−2229.6357
Electron affinity (*A*)	0.1509	0.1262	0.2222	0.2241	0.1179	0.2269	0.2282
Negative chemical potential (−μ)	0.1807	0.1669	0.2839	0.2843	0.1681	0.2813	0.2814
Chemical hardness (η)	0.0298	0.0505	0.0616	0.0601	0.0502	0.0544	0.0532
Global electrophilicity (ω)	0.5482	0.2758	0.6542	0.6718	0.2814	0.7275	0.7444
Mulliken charge on M	0.461	0.539	0.732	0.647	0.838	0.630	1.041

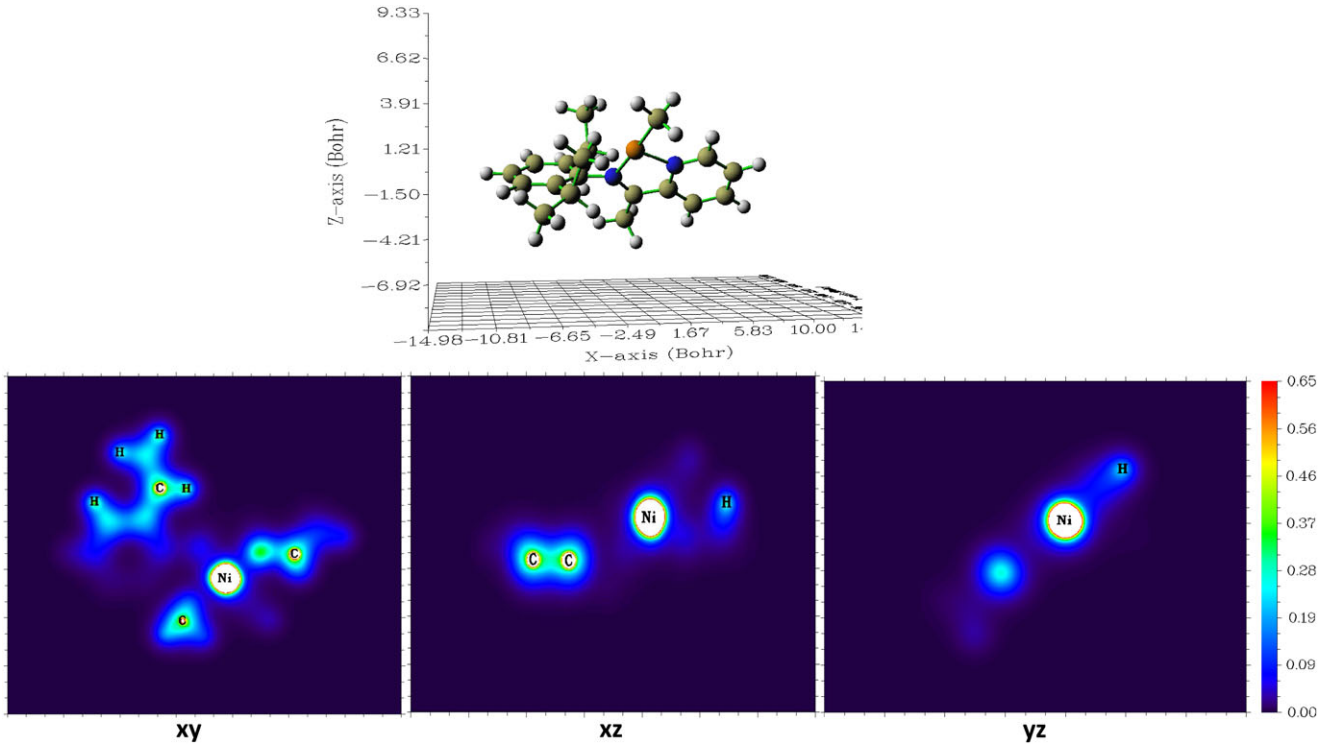

Figure 3. Three-dimensional structure of Ni-MCC and electron density graphs in each plane (*xy*, *xz*, and *yz*) containing a Ni center. [Color figure can be viewed at wileyonlinelibrary.com]

higher values than that of the polyethylene samples produced with the **N** and **F** catalysts individually. This might be due to the synergistic effect of the active centers, hindering β-hydrogen transfer, and a higher propagation/termination rate.[49] As shown in Table II, $\overline{M}_v$ of the resultant polyethylene blends increased to 19.4×10^4 (entry 4, Table II) by increasing the molar fraction of

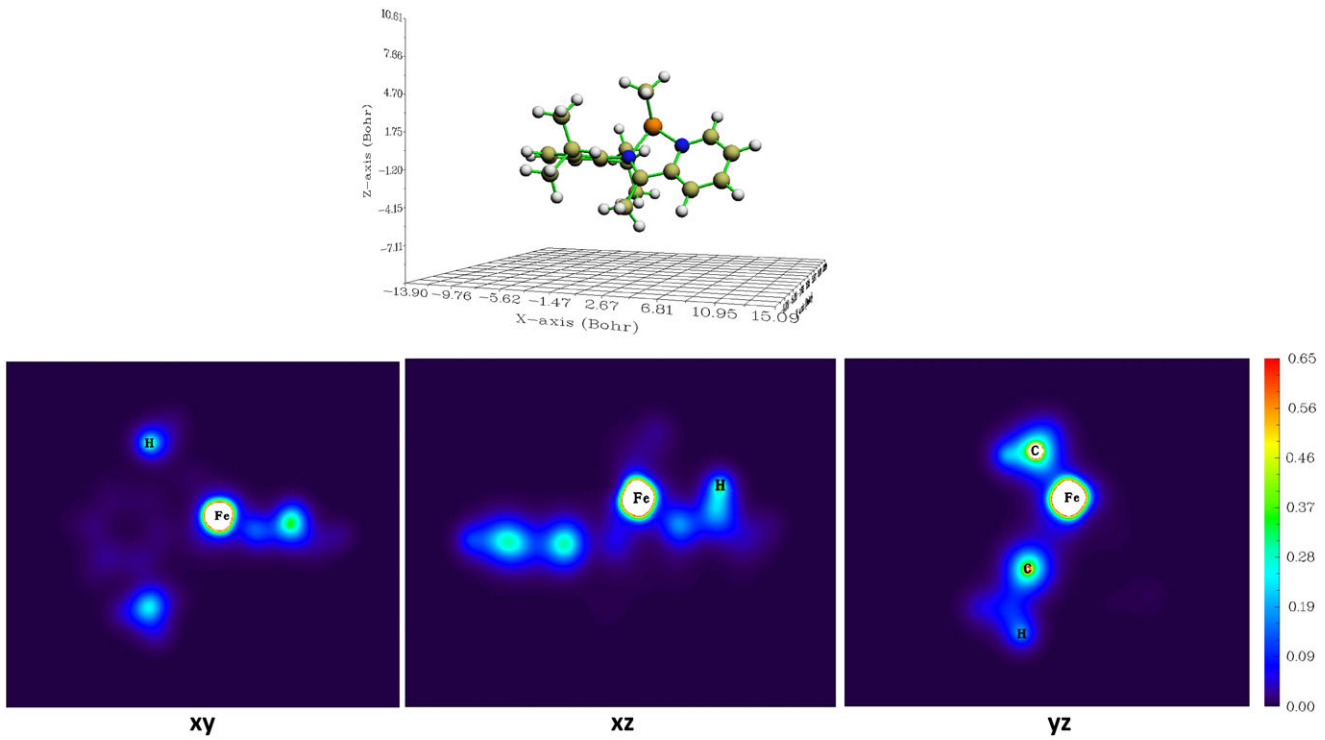

Figure 4. Three-dimensional structure of Fe-MCC and electron density graphs in each plane (*xy*, *xz*, and *yz*) containing an Fe center. [Color figure can be viewed at wileyonlinelibrary.com]

Table II. Results of Ethylene Polymerization Using the Binary Catalytic Systems

Entry	Cat N:Cat F	Activity[a]	M_v[b]	T_m (°C)[c]	X_C (%)[c]	VC[d]	BD[e]
1	100:0 (10 μmol Ni)	3.50	0.90	91.60, 70	2.05, 2.30	3.93	115.4
2	70:30 (7 μmol Ni: 3 μmol Fe)	5.05	12.5	91.20	2.37	3.17	104.0
3	50:50 (5 μmol Ni: 5 μmol Fe)	7.50	4.4	127.80, 105.40	3.20, 41.29	1.87	35.9
4	30:70 (3 μmol Ni: 7 μmol Fe)	12.60	19.4	113.40, 99.10	8.80, 16.77	2.75	83.3
5	0:100 (10 μmol Fe)	33.33	1.2	105.10	28.55	4.94	9.2

Conditions: toluene = 100 mL, polymerization temperature = 0 °C, ethylene pressure = 1.2 bar, polymerization time = 2 h, MMAO as cocatalyst, [Al]/[M] = 1200.
[a] Activity × 10^4 g (PE) mol (Ni+Fe)$^{-1}$ h^{-1}.
[b] Viscosity average molecular weight, ×10^4.
[c] Determined by DSC[47].
[d] Vinyl content: determined by FTIR,[40] number of vinyl groups/1000 carbon atoms.
[e] Branching density: determined by FTIR,[46] methyl branches/1000 carbon atoms.

catalyst F in the catalyst combination. Figure 5 shows the broadened melting area of the polymers obtained with the N/F/MMAO system. It also shows an increase in the branching content of the polyethylene sample synthesized by catalyst **N**, which led to a shift in the melting and crystallization peaks toward lower temperatures and a broadening compared to those in polyethylene obtained by catalyst **F**.[7] Furthermore, the melting temperature of the polymers obtained from the N/F/MMAO systems increased as the [Fe]/[Ni] ratio increased. Therefore, by increasing the X_F from 30% to 70% in the catalyst combination, virtually two separate melting points are observed. The two melting peaks of the samples implied a melting–recrystallization mechanism; such behavior has also been observed and discussed in similar systems.[40,49,50]

However, the highest and lowest melting point areas as well as degree of crystallinity of the polymers produced using different catalyst combinations were assigned to the samples produced at fixed 50:50 and 30:70 [Ni]/[Fe] proportions (entries 3 and 4, Table II), respectively. It seems that the polyethylene blend prepared using 50% X_F is an appropriate composition for the desired reactor blend in regard to polymer processing. Among all the obtained products, this sample showed the lowest branching (see Table II) and vinyl end content (35.9 methyl branches/1000 carbon atoms and 1.87 vinyl groups/1000 carbon atoms, respectively).

As shown in Table II, the lowest degree of branching and the highest vinyl end content among the resultant samples (4.94 vinyl groups/1000 carbon atoms) belonged to the sample produced by the catalyst **F** (9.2 methyl branches/1000 carbon atoms), which can attributed to the lower tendency of Fe for chain walking and reinsertion of macromonomer, leading to a higher linearity in the polyolefin.[51]

Morphology of the Polyethylene Blends

The SEM images were used to monitor the influence of different catalyst combinations on the structural morphology of the resultant products. The images are depicted in Figure 6. As can be

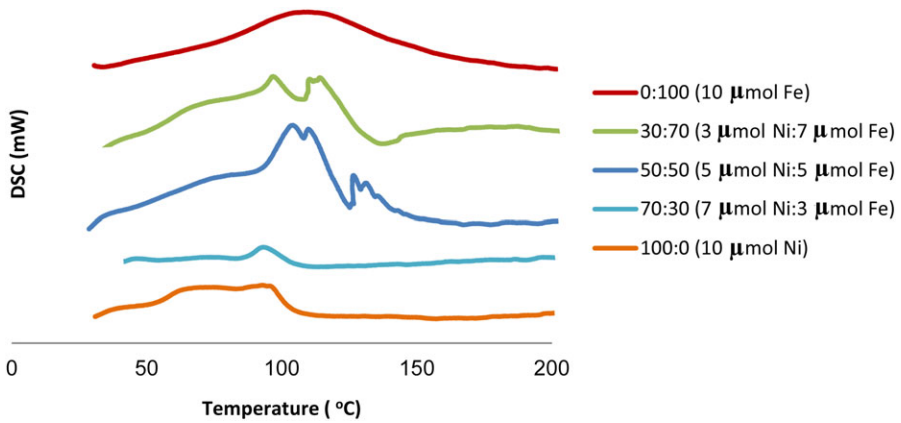

Figure 5. DSC thermograms of polyethylene obtained using the N/F/MMAO binary system at 0 °C: the effect of X_N on polymer melting behavior. [Color figure can be viewed at wileyonlinelibrary.com]

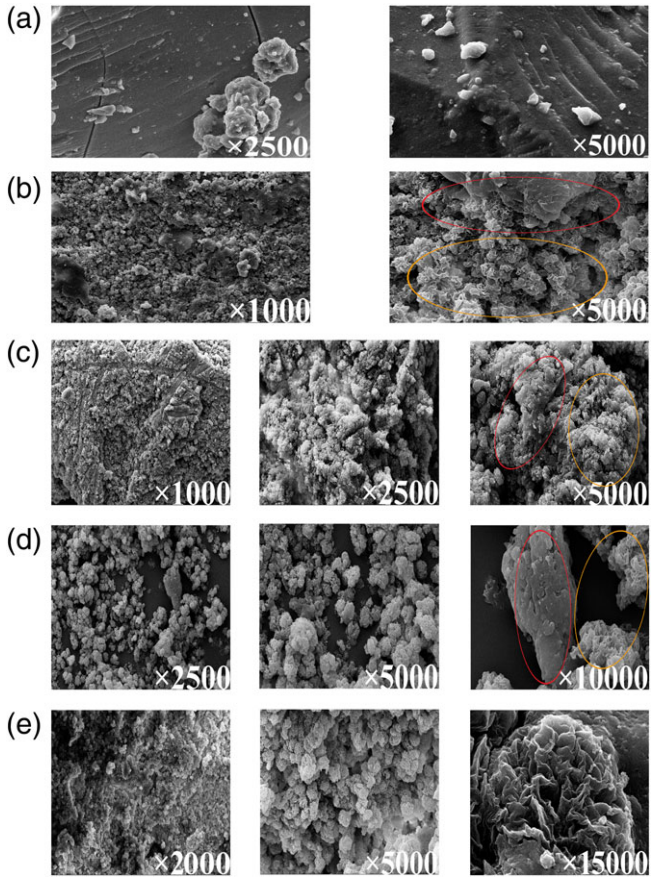

Figure 6. SEM images of polyethylene prepared with different nickel molar fractions (X_N) in the N/F/MMAO binary system: (a) 0, (b) 0.3, (c) 0.5, (d) 0.7, (e) 1. [Color figure can be viewed at wileyonlinelibrary.com]

seen, a uniform morphology is observed for the samples obtained using the catalysts **N** and **F** individually. The morphologies observed for the samples were cauliflower [Figure 6(e)] and amorphous [Figure 6(a)]. However, by increasing the molar fraction of catalyst **F** in the catalyst combination, the uniform morphology disappeared as the amorphous phase in the total structure of the resultant polyethylene blends increased. The DSC thermograms showed two dominant crystal peaks of the polyethylene, corresponding to the distinct polymerization process from the active centers as well as the existence of two distinct phases in the SEM images (Figures 5 and 6). However, it is not possible to distinguish the presence of two polymer phases in the SEM images of the polyethylene blend obtained using the 50:50 [Ni]/[Fe] molar fraction in the catalyst combination, which can be attributed to the different interaction and good miscibility between the polyethylene phases produced [Figure 6(c)].

Thermal and Structural Analysis of LDPE/Nanocomposites

The binary catalyst system based on the pyridine-imine nickel and iron catalysts (**N**:**F**) was used to produce nanocomposites. The influence of type and content of MWCNT on the catalytic activity was investigated. The polymerization was carried out in the presence of the binary system (5 mmol **F** and 5 mmol **N**) at 0 °C and 2 bar of monomer for 3 h. The nanocomposite samples were analyzed, and the details are gathered in Table III.

The catalytic activity slightly decreased with low amounts of both sizes of MWCNTs, consistent with previous results.[24,28,52] These values were in the range of 0.66×10^4 to 4.00×10^4 [g (PE) mol $(Fe+Ni)^{-1}$ h^{-1}]. This observation might be attributed to the deactivation of active polymerization sites by the naturally occurring functional groups on the surface of the CNTs.[28] However, the presence of impurity as an obstacle for ethylene monomer diffusion and reaching the active center cannot be ignored.[53] On the other hand, as the $MWCNT_{20\text{-}30}$ content was increased in the polymerization media, the activity of the catalysts improved [from 1.00×10^4 to 4.00×10^4 g (PE) mol $(Fe+Ni)^{-1}$ h^{-1}], in which a distribution of active centers through a direct adsorption of these catalysts onto the surface of nanotubes can be suggested.[18,53] In contrast, the MWCNTs with larger diameter (30–50 nm) led to a frustrating effect on catalyst productivity in the polymerization of ethylene (entries 4 and 5, Table III).

As shown in Figure 7, the prepared LDPE/nanocomposites exhibited a lower degree of crystallinity and melting point than the neat polyethylene blend (entries 3 and 4, Table III), and these numerous differences in the LDPE/nanocomposites containing

Table III. *In Situ* Polymerization Results for Production of LDPE/Nanocomposites Using a Combination of Pyridine-imine Catalysts Based on Nickel (**N**) and Iron (**F**)

Entry	wt %[a]	MWCNT type	Content (mg)	Time (min)	PE (g)	Activity[b]	T_m (°C)[c]	X_C (%)[c]	VC[d]	BD[e]
1	0	—	0	120	1.51	7.50	127.80, 105.40	3.20, 41.30	1.87	35.9
2	2.33	20–30 nm	7	180	0.30	1.00	n.d.	n.d.	0.93	50.1
3	1.80	20–30 nm	21	180	1.17	4.00	121.90, 102.70	0.83, 4.53	0.12	34.7
4	0.87	30–50 nm	7	180	0.80	2.70	87.60, 52.20	2.30, 0.40	4.17	70.8
5	10.50	30–50 nm	21	180	0.20	0.66	n.d.	n.d.	5.30	11.5

Conditions: toluene = 100 mL, polymerization temperature = 0 °C, ethylene pressure = 1.2 bar, catalyst **N** = 5 μmol, catalyst **F** = 5 μmol (50:50), MMAO as cocatalyst, [Al]/[M]= 1200.
[a] wt % of CNT in polymer matrix.
[b] Activity $\times 10^4$ g (PE) mol $(Ni+Fe)^{-1}$ h^{-1}.
[c] Determined by DSC.[47]
[d] Vinyl content: determined by FTIR,[40] number of vinyl groups/1000 carbon atoms.
[e] Branching density: determined by FTIR,[46] methyl branches/1000 carbon atoms.

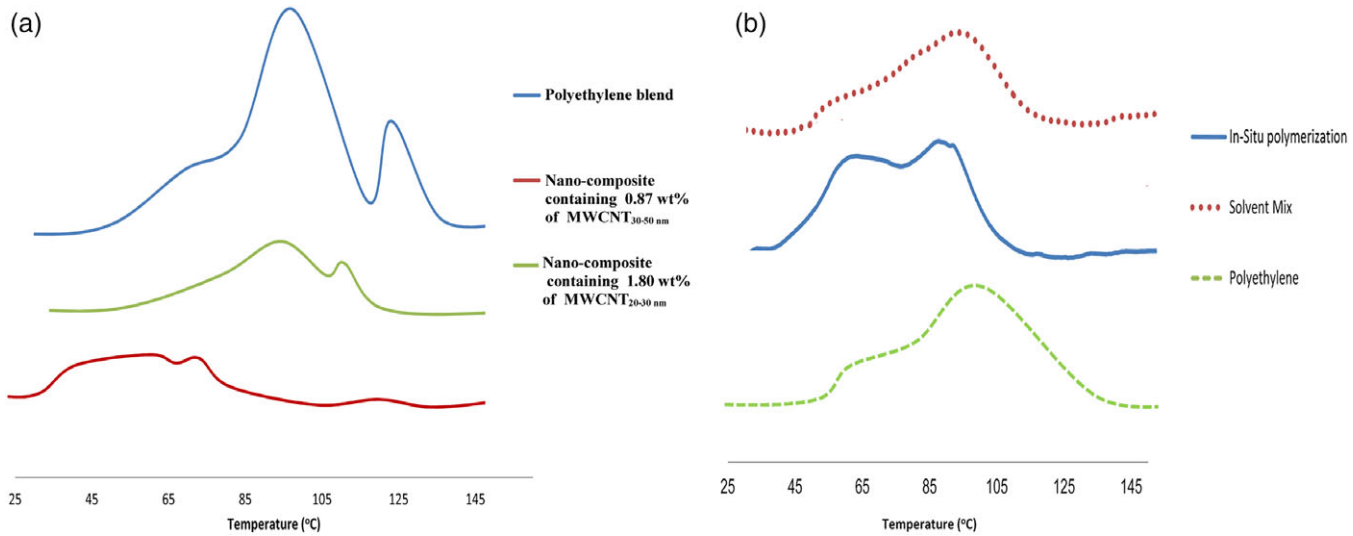

Figure 7. DSC thermograms of the resultant LDPE/nanocomposites using (a) a combination of pyridine-imine catalysts based on nickel (**N**) and iron (**F**) via *in situ* polymerization; (b) via *in situ* and solution-mixing method. [Color figure can be viewed at wileyonlinelibrary.com]

$MWCNT_{30\text{-}50}$ can be ascribed to a high degree of branching (70.8 methyl branch/1000 carbon atoms; entry 1, Table III).[54] In fact, the nanofiller (such as CNTs) could increase the chain transfer reaction and β-hydrogen elimination due to an electronic effect that consequently increases the branching content.[23,24] As exhibited in Figure 8 and Table III (Entries 2–5), the values for LDPE/nanocomposite samples varied between 11.5 and 70.8 methyl branches/1000 carbon atoms. Furthermore, nanocomposite samples containing $MWCNT_{20\text{-}30}$ showed the lowest vinyl content (0.12 vinyl groups/1000 carbon atoms) among all the samples. However, the addition of $MWCNT_{30\text{-}50}$ into the polymerization media led to a greater vinyl content in the products, up to 5.30 vinyl groups/1000 carbon atoms.

In order to better understand the effect of MWCNTs on the final properties of LDPE/nanocomposites, the polymerization of ethylene using a single Ni catalyst and MWCNT was carried out, and the results are gathered in Table IV.

The activity of the catalyst **N** in polymerization, as well as the melting point and crystallinity of the resultant sample, dropped as the $MWCNT_{20\text{-}30}$ was added into the polymerization reactor. However, the branching and vinyl content trends in these

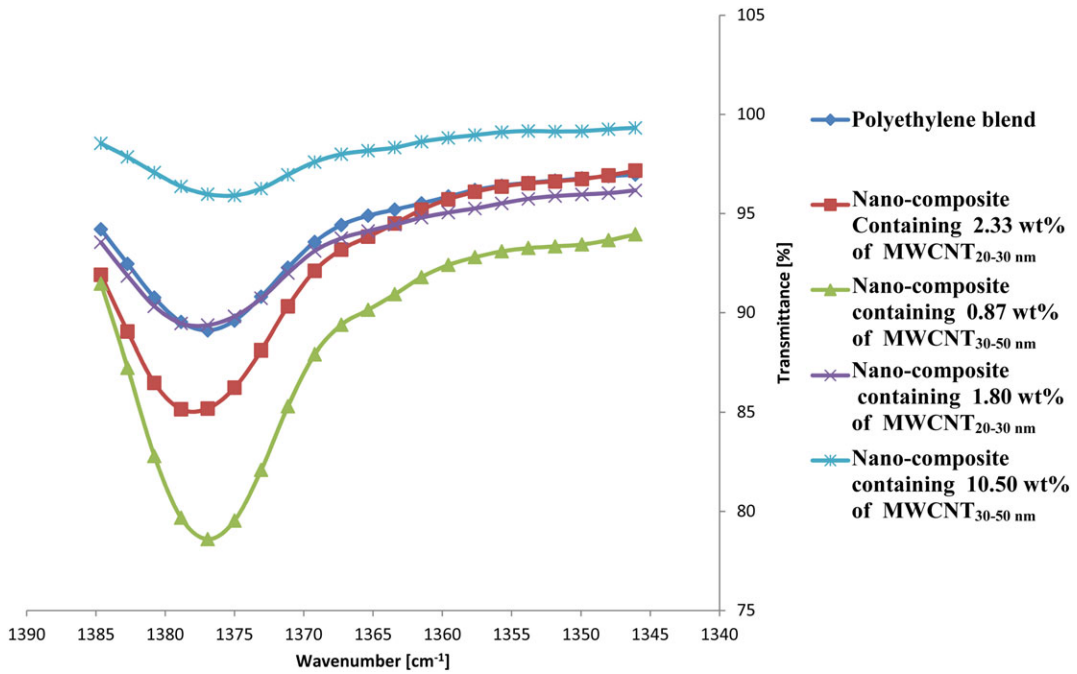

Figure 8. Difference spectra of the methyl symmetrical deformation band for the resultant LDPE/nanocomposites that used a combination of pyridine-imine catalysts based on nickel (**N**) and iron (**F**) (magnification of the 1300–1400 cm^{-1} range). [Color figure can be viewed at wileyonlinelibrary.com]

Table IV. LDPE/Nanocomposites Prepared through *in Situ* Polymerization and Solution-Mixing Techniques

Entry	Method	PE (g)	Time (min)	Content (mg)	wt (%)[a]	Activity[b]	T_m (°C)[c]	X_C (%)[c]	VC[d]	BD[e]
1	*in situ*	3.62	120	0	0	18.10	102.60	30.40	5.26	68.8
2	*in situ*	2.00	180	5	0.25	6.60	n.d.	n.d.	5.63	132.3
3	*in situ*	2.25	180	10	0.44	7.50	64.40, 89.90	2.83, 3.01	4.55	104.1
4	Solution mixing[f]	—	—	2	0.44	—	94.80	7.20	—[g]	—[g]

Polymerization conditions: toluene = 100 mL, polymerization temperature = 0 °C, ethylene pressure = 2 bar, catalyst **N** = 10 μmol, MMAO as cocatalyst, [Al]/[M]= 1000; n.d. = no data.
[a] wt % of $MWCNT_{20\text{-}30}$ in polymer matrix.
[b] Activity × 10^4 g (PE) mol (Ni)$^{-1}$ hr^{-1}.
[c] Determined by DSC.[47]
[d] Vinyl content: determined by FTIR,[40] number of vinyl groups/1000 carbon atoms.
[e] Branching density: [d]etermined by FTIR,[46] methyl branches/1000 carbon atoms.
[f] Prepared by instruction in 0.45 g of LDPE (entry 1).[37]
[g] Similar to LDPE sample.

samples are not the same as in the sample produced by the dual catalyst system under the same conditions. The result is consistent with the fact that the catalyst **F** is more dominant than catalyst **N** in relation to the sample properties (entries 2 and 3, Tables III and IV). As shown in Figure 7(b), the sample obtained using the *in situ* polymerization technique indicated a lower melting temperature as well as crystallinity than found for the corresponding nanocomposite obtained via solution mixing (entries 2–4, Table IV). This behavior can be explained by the higher degree of branching and weaker intermolecular forces in the resultant sample as compared to the sample obtained by solution mixing and the possible interaction of MWCNTs during *in situ* polymerization.[10,28]

Morphology of LDPE/Nanocomposites

SEM images were used to investigate the influence of the different type and content of MWCNTs as well as different preparation techniques on the morphology of the final products.

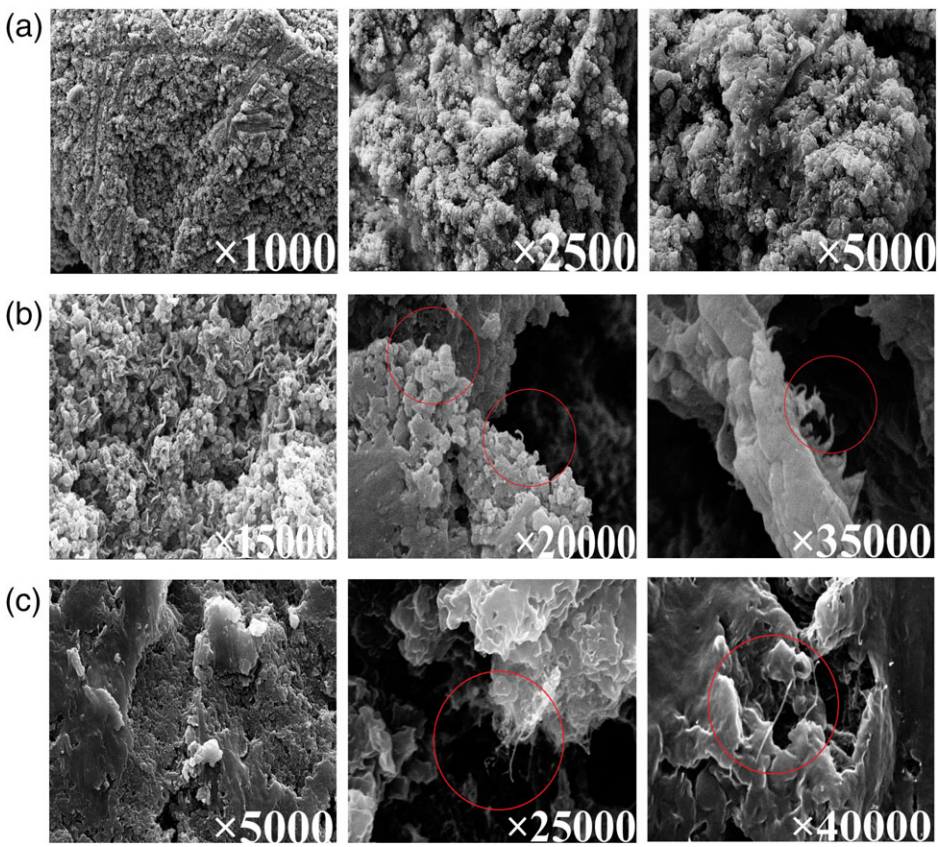

Figure 9. SEM images of (a) polyethylene blend, and LDPE/nanocomposites containing (b) $MWCNT_{20\text{-}30}$ (1.80 wt %) and (c) $MWCNT_{30\text{-}50}$ (0.87 wt %). [Color figure can be viewed at wileyonlinelibrary.com]

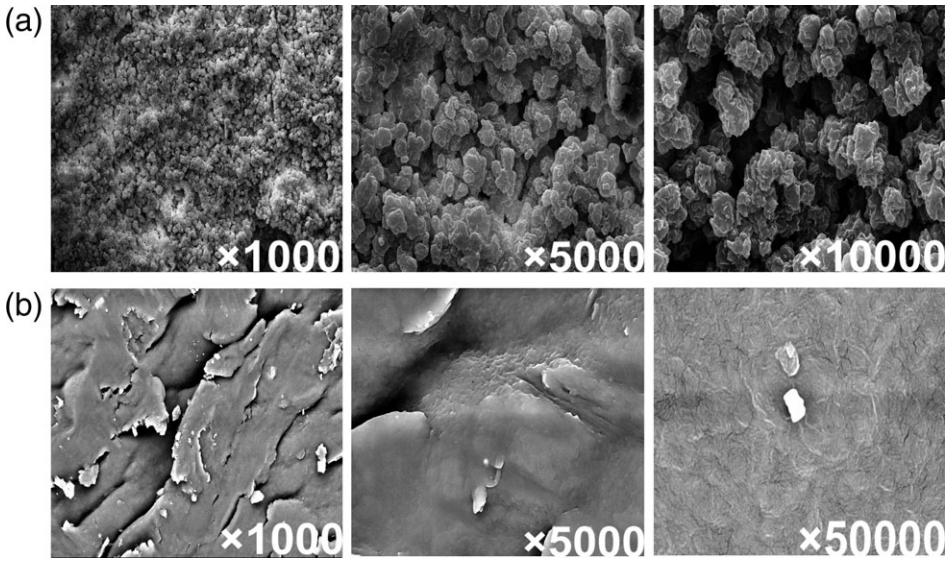

Figure 10. SEM images of LDPE/nanocomposites prepared via (a) *in situ* polymerization and (b) solution-mixing method.

Therefore, the samples along with their dispersity are depicted in Figures 9 and 10. In Figure 9(b), a uniform morphology is not seen for the sample obtained in the presence of $MWCNT_{20\text{-}30}$ (entry 3, Table III); however, virtually a single fraction of the crystalline phase in DSC traces was observed for the sample containing $MWCNT_{30\text{-}50}$ [entry 5, Table III, and Figure 7(a)], in which the presence of nanotubes is obvious in the polymer matrix [Figure 9(c)].

In Figure 10(b), a soft, uniform morphology without any specific shape can be observed for the sample prepared via the solution-mixing technique, and a broad single peak is obtained in the DSC thermogram [Figure 7(b)]. In contrast, two melting peaks are more distinguishable and different crystalline phases in the DSC trace [Figure 7(b)] were recorded for the sample with a uniform morphology prepared by the *in situ* polymerization technique [Figure 9(a)].

Thermogravimetric Analysis

TGA is a useful tool for evaluating the thermal stability of the nanocomposite samples. The resulting thermogravimetric studies are shown in Figure 11 and Table V. The thermal stability of the nanocomposite samples strongly depends on the type and content of CNTs. At the same conditions, the lowest and highest half-lives of the nanocomposites were attributed to those products, respectively, in the presence of 1.80 wt % $MWCNT_{20\text{-}30}$ (entry 2, Table V) and 10.50 wt % $MWCNT_{30\text{-}50}$ (entry 4, Table V). The differential curve analysis of the resultant samples (Table V) showed that the sample with a high content of

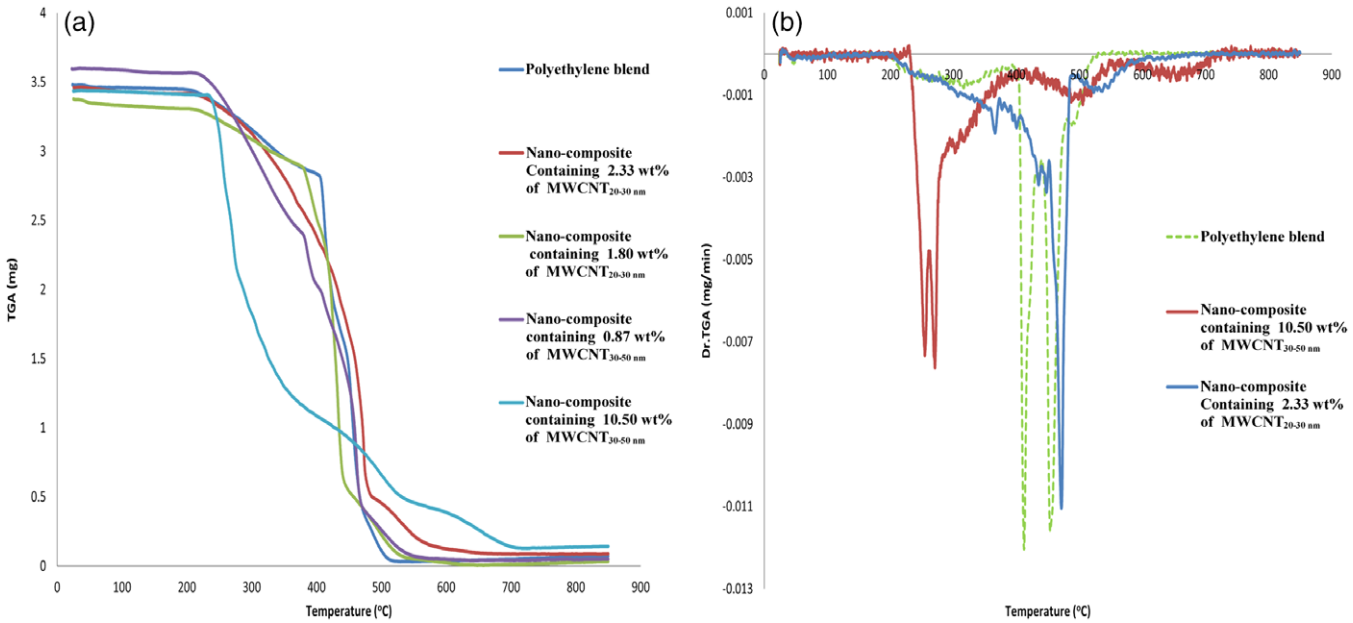

Figure 11. Thermogravimetric (a) and differential thermogravimetric (b) curves of the neat polyethylene blend and LDPE/nanocomposites prepared by *in situ* polymerization. [Color figure can be viewed at wileyonlinelibrary.com]

Table V. Differential Thermogravimetric Results for LDPE/Nanocomposites Prepared by *in Situ* Polymerization

Entry	wt %[a]	Content of CNT (mg)	Diameter of CNT (nm)	Degradation data	Time (s)	Temperature (°C)	Half-life (s)
1	2.33	7	20–30	Onset	1069	194.04	2368
				Peak	2727	471.55	
				End	3784	647.70	
2	1.80	21	20–30	Onset	1000	198.33	2588
				Peak	2399	432.25	
				End	2533	618.05	
3	0.87	7	30–50	Onset	1016	187.92	2389
				Peak	2184, 2642	384.48, 461.51	
				End	3310	573.96	
4	10.50	21	30–50	Onset	1219	217.74	1755
				Peak	1435, 1529	254.44, 270.41	
				End	4152	708.71	
5	0	0	—	Onset	1019	187	2510
				Peak	2372, 2621	453.30, 411.90	
				End	3045	523.77	

[a] wt % of MWCNT in polymer matrix.

$MWCNT_{30\text{-}50}$ (10.50 wt %) has the highest onset and end point of degradation temperature (entry 4, Table V). However, the greatest weight loss in this sample occurred at 10.66% of the degradation time (entry 4, Table V). Furthermore, a single peak is also obtained for the nanocomposite in the presence of $MWCNT_{20\text{-}30}$ (2.33 wt %), which had a higher combustion temperature (647.7 °C) than the neat polyethylene blend [Figure 11 (b)]. In fact, with decreasing $MWCNT_{20\text{-}30}$ content (from 2.33 to 1.80 wt %), the thermal stability of the obtained nanocomposites slightly increased, which can be attributed to the increasing amount of crystallinity and decrease in branching content in the prepared sample.[55]

CONCLUSIONS

Reactor blends containing linear and highly branched polyethylene were prepared in the presence of modified methylaluminoxane using a binary system based on pyridine-imine nickel (**N**) and iron (**F**) catalysts. As a result, introducing different ratios of the catalysts at the same conditions can enhance the properties of the obtained products such as $\overline{M}_v$ as well as the thermal properties [up to 19.4×10^4 g (PE) mol $(Fe+Ni)^{-1}$ h^{-1} and 127.8 °C]. The DSC and SEM results indicate that the combination of linear PE with less branched PE through the binary catalyst system can achieve a better polymer miscibility when polymerization is conducted at a fixed 50:50 [Ni]/[Fe] molar ratio of the catalysts. LDPE/nanocomposite samples containing different types and content of MWCNTs were successfully prepared via *in situ* polymerization. By increasing the content of $MWCNT_{20\text{-}30}$, the activity of the catalysts was improved, which can be attributed to adsorption of catalyst on the CNT surface, but overall the performance of the catalyst mixture decreased in the presence of MWCNTs. The LDPE/nanocomposites with lower melting point and degree of crystallinity compared to the neat polyethylene blend implied higher chain walking, degree of branching, and vinyl content. Moreover, the sample containing $MWCNT_{20\text{-}30}$ exhibited contrary results in regard to the unsaturation content. The melting point and crystallinity extent of the samples obtained via the *in situ* process exhibited lower values as well as a distinct morphology compared to the corresponding sample prepared by the solution-mixing technique. The addition of $MWCNT_{20\text{-}30}$ caused an increase in the thermal stability, due to a better and uniform dispersion of the nanofillers in the LDPE matrix.

ACKNOWLEDGMENTS

This research was financially supported by a grant from Ferdowsi University of Mashhad (FUM, grant 3/39813).

REFERENCES

1. Kaminsky, W. *Materials*. **2014**, *7*, 1995.
2. Park, S.; He, S.; Wang, J.; Stein, A.; Macosko, C. W. *Polymer*. **2016**, *104*, 1.
3. AlObaidi, F.; Zhu, S. *J. Appl. Polym. Sci.* **2005**, *96*, 2212.
4. Long, Y. Y.; Liu, S. R.; Cui, L.; Li, Y. S. *J. Appl. Polym. Sci.* **2010**, *115*, 3045.
5. Bianchini, C.; Frediani, M.; Giambastiani, G.; Kaminsky, W.; Meli, A.; Passaglia, E. *Macromol. Rapid Commun.* **2005**, *26*, 1218.
6. Ahmadi, M.; Jamjah, R.; Nekoomanesh, M.; Zohuri, G. H.; Arabi, H. *Macromol. React. Eng.* **2007**, *1*, 604.

7. Ahmadjo, S.; Dehghani, S.; Zohuri, G. H.; Nejabat, G. R.; Jafarian, H.; Ahmadi, M.; Mortazavi, S. M. M. *Macromol. React. Eng.* **2015**, *9*, 8.
8. Cho, H. S.; Chung, J. S.; Lee, W. Y. *J. Mol. Catal. A: Chem.* **2000**, *159*, 203.
9. Mortazavi, S. M. M.; Jafarian, H.; Ahmadi, M.; Ahmadjo, S. *J. Therm. Anal. Calorim.* **2016**, *123*, 1469.
10. Pan, L.; Zhang, K. Y.; Li, Y. G.; Bo, S. Q.; Li, Y. S. *J. Appl. Polym. Sci.* **2007**, *104*, 4188.
11. Ferreira, A. E.; Cerrada, M. L.; Pérez, E.; Lorenzo, V.; Vallés, E.; Ressia, J.; Cramail, H.; Lourenço, J. P.; Ribeiro, M. R. *eXPRESS Polym. Lett.* **2017**, *11*, 344.
12. Santos, J. C. S. D.; Barbosa, O.; Ortiz, C.; Berenguer-Murcia, A.; Rodrigues, R. C.; Fernandez-Lafuente, R. *Chem. Cat. Chem.* **2015**, *7*, 2413.
13. Guo, C. Y.; Xu, H.; Zhang, M.; Yang, H. J.; Yana, F.; Yuana, G. *Polym. Int.* **2010**, *59*, 725.
14. Xu, H.; Guo, C. Y.; Zhang, M.; Yang, H. J.; Dong, J.; Yuan, G. *Catal. Commun.* **2007**, *8*, 2143.
15. Bredeau, S.; Peeterbroeck, S.; Bonduel, D.; Alexandre, M.; Dubois, P. *Polym. Int.* **2008**, *57*, 547.
16. Kittelson, D. B. *J. Aerosol Sci.* **1998**, *29*, 575.
17. Badaire, S.; Poulin, P.; Maugey, M.; Zakri, C. *Langmuir*. **2004**, *20*, 10367.
18. Vaisman, L.; Wagner, H. D.; Marom, G. *Adv. Colloid Interface Sci.* **2006**, *128*, 37.
19. Sun, Y. P.; Fu, K.; Lin, Y.; Huang, W. *Acc. Chem. Res.* **2002**, *35*, 1096.
20. Baskaran, D.; Mays, J. W.; Bratcher, M. S. *Angew. Chem. Int. Ed.* **2004**, *43*, 2138.
21. Kong, H.; Gao, C.; Yan, D. *J. Am. Chem. Soc.* **2004**, *126*, 412.
22. Funck, A.; Kaminsky, W. *Compos. Sci. Technol.* **2007**, *67*, 906.
23. Boggioni, L.; Scalcione, G.; Ravasio, A.; Bertini, F.; Arrigo, C. D.; Tritto, I. *Macromol. Chem. Phys.* **2012**, *213*, 627.
24. Zhang, L.; Yue, E.; Liu, B.; Serp, P.; Redshaw, C.; Sun, W. H.; Durand, J. *Catal. Commun.* **2014**, *43*, 227.
25. Kim, J.; Hong, S. M.; Kwak, S.; Seo, Y. *Phys. Chem. Chem. Phys.* **2009**, *11*, 10851.
26. Trujillo, M.; Arnal, M. L.; Müller, A. J.; Bredeau, S.; Bonduel, D.; Dubois, P.; Hamley, I. W.; Castelletto, V. *Macromolecules*. **2008**, *41*, 2087.
27. Pinheiro, A. C.; Casagrande, A. C.; Casagrande, O. L. *J. Polym. Sci., Part A: Polym. Chem.* **2014**, *52*, 3506.
28. Khoshsefat, M.; Ahmadjo, S.; Mortazavi, S. M. M.; Zohuri, G. H. *RSC Adv.* **2016**, *6*, 88625.
29. Park, S.; Yoon, S. W.; Choi, H.; Lee, J. S.; Cho, W. K.; Kim, J.; Park, H. J.; Yun, W. S.; Choi, C. H.; Do, Y.; Choi, I. S. *Chem. Mater.* **2008**, *20*, 4588.
30. Zhang, L.; Castillejos, E.; Serp, P.; Sun, W. H.; Durand, J. *Catal. Today*. **2014**, *235*, 33.
31. Bin, Y.; Kitanaka, M.; Zhu, D.; Matsuo, M. *Macromolecules*. **2003**, *36*, 6213.
32. Chen, Q.; Bin, Y.; Matsuo, M. *Macromolecules*. **2006**, *39*, 6528.
33. Xiao, K. Q.; Zhang, L. C.; Zarudi, I. *Compos. Sci. Technol.* **2007**, *67*, 177.
34. Haggenmueller, R.; Guthy, C.; Lukes, J. R.; Fischer, J. E.; Winey, K. I. *Macromolecules*. **2007**, *40*, 2417.
35. Khanam, P. N.; AlMaadeed, M. A.; Ouederni, M.; Harkin-Jones, E.; Mayoral, B.; Hamilton, A.; Sun, D. *Vacuum*. **2016**, *130*, 63.
36. McNally, T.; Pötschke, P.; Halley, P.; Murphy, M.; Martin, D.; Bell, S. E.; Brennan, G. P.; Bein, D.; Lemoine, P.; Quinn, J. P. *Polymer*. **2005**, *46*, 8222.
37. Liao, M.; Zhu, J.; Xu, H.; Li, Y.; Shan, W. *J. Appl. Polym. Sci.* **2004**, *92*, 3430.
38. Valentini, L.; Biagiotti, J.; Kenny, J. M.; Santucci, S. *Compos. Sci. Technol.* **2003**, *63*, 1149.
39. Sangokoya, S. A. Eur. Pat. EP0463555 B1 (**1996**).
40. Mogheiseh, M.; Zohuri, G. H.; Khoshsefat, M. *Macromol. React. Eng*. **2018**, *12*, 1800006.
41. Khoshsefat, M.; Zohuri, G. H.; Ramezanian, N.; Ahmadjo, S.; Haghpanah, M. *J. Polym. Sci. Polym. Chem.* **2016**, *54*, 3000.
42. Kong, Y.; Hay, J. N. *Polymer*. **2002**, *43*, 3873.
43. Laine, T. V.; Piironen, U.; Lappalainen, K.; Klinga, M.; Aitola, E.; Leskelä, M. J. *J. Organomet. Chem.* **2000**, *606*, 112.
44. Nienkemper, K.; Kotov, V. V.; Kehr, G.; Erker, G.; Fröhlich, R. *Eur. J. Inorg. Chem.* **2006**, *2*, 366.
45. Yang, P.; Yang, Y.; Zhang, C.; Yang, X. J.; Hu, H. M.; Gao, Y.; Wu, B. *Inorg. Chim. Acta*. **2009**, *362*, 89.
46. Bezerra, R. M.; Neto, D. M. A.; Galvão, W. S.; Rios, N. S.; Carvalho, A. C. L. D. M.; Correa, M. A.; Bohn, F.; Fernandez-Lafuente, R.; Fechine, P. B.; de Mattos, M. C.; dos Santos, J. C. *Biochem. Eng. J.* **2017**, *125*, 104.
47. Mogheiseh, M.; Zohuri, G. H.; Yazdanbakhsh, M. Presented at the 1st Iranian Applied Chemistry Seminar (1IACS), Tabriz, Iran, **August 2016**.
48. Kimiaghalam, M.; Isfahani, H. N.; Zohuri, G. H.; Keivanloo, A. *Appl. Organomet. Chem.* **2018**, *32*, e4153.
49. Li, W.; Wang, J.; Jiang, B.; Yang, Y.; Jie, Z. *Polym. Int.* **2010**, *59*, 617.
50. Yeh, J. T.; Chang, S. S.; Wu, T. W. *J. Appl. Polym. Sci.* **2008**, *107*, 854.
51. Pourtaghi-Zahed, H.; Zohuri, G. H. *Polym. Bull.* **2013**, *70*, 1769.
52. Kimiaghalam, M.; Isfahani, H. N.; Zohuri, G. H.; Keivanloo, A. *Inorg. Chim. Acta*. **2017**, *464*, 99.
53. Toti, A.; Giambastiani, G.; Bianchini, C.; Meli, A.; Bredeau, S.; Dubois, P.; Bonduel, D.; Claes, M. *Chem. Mater.* **2008**, *20*, 3092.
54. Ye, Z. B.; Alsyouri, H.; Zhu, S. P.; Lin, Y. S. *Polymer*. **2003**, *44*, 969.
55. Singh, B. P.; Saini, P.; Gupta, T.; Garg, P.; Kumar, G.; Pande, I.; Pande, S.; Seth, R. K.; Dhawan, S. K.; Mathur, R. B. *J. Nanopart. Res.* **2011**, *13*, 7065.